Gas-surface interactions using accommodation coefficients for a dilute and a dense gas in a micro- or nanochannel: Heat flux predictions using combined molecular dynamics and Monte Carlo techniques

S. V. Nedea* and A. A. van Steenhoven
Department of Mechanical Engineering, Eindhoven University of Technology, P.O. Box 513, 5600MB Eindhoven, the Netherlands

A. J. Markvoort and P. Spijker
Biomedical Engineering, Eindhoven University of Technology, P.O. Box 513, 5600MB Eindhoven, the Netherlands

D. Giordano
European Space Agency, 2200AG Noordwijk, the Netherlands

(Received 22 February 2013; revised manuscript received 14 February 2014; published 14 May 2014)

The influence of gas-surface interactions of a dilute gas confined between two parallel walls on the heat flux predictions is investigated using a combined Monte Carlo (MC) and molecular dynamics (MD) approach. The accommodation coefficients are computed from the temperature of incident and reflected molecules in molecular dynamics and used as effective coefficients in Maxwell-like boundary conditions in Monte Carlo simulations. Hydrophobic and hydrophilic wall interactions are studied, and the effect of the gas-surface interaction potential on the heat flux and other characteristic parameters like density and temperature is shown. The heat flux dependence on the accommodation coefficient is shown for different fluid-wall mass ratios. We find that the accommodation coefficient is increasing considerably when the mass ratio is decreased. An effective map of the heat flux depending on the accommodation coefficient is given and we show that MC heat flux predictions using Maxwell boundary conditions based on the accommodation coefficient give good results when compared to pure molecular dynamics heat predictions. The accommodation coefficients computed for a dilute gas for different gas-wall interaction parameters and mass ratios are transferred to compute the heat flux predictions for a dense gas. Comparison of the heat fluxes derived using explicit MD, MC with Maxwell-like boundary conditions based on the accommodation coefficients, and pure Maxwell boundary conditions are discussed. A map of the heat flux dependence on the accommodation coefficients for a dense gas, and the effective accommodation coefficients for different gas-wall interactions are given. In the end, this approach is applied to study the gas-surface interactions of argon and xenon molecules on a platinum surface. The derived accommodation coefficients are compared with values of experimental results.

DOI: 10.1103/PhysRevE.89.053012 PACS number(s): 47.45.Ab, 47.61.−k, 47.11.Mn, 47.45.Gx

I. INTRODUCTION

Energy transfer in the gas-surface interface plays a very important role in many practical areas as corrosion, plasma confinement, catalysis, and heat transfer. Studying the gas-surface interactions at an atomistic level can provide essential information on molecular behavior next to the surface and on the energy exchange in this interface.

Heat transfer at an atomistic level became one of the most important issues within the microfluidics field, for instance, in microchannel cooling applications. As a lot of electronic components produce heat when operating, cooling these devices is essential for the long lifetime of these components. These devices can be cooled locally where the power is produced using a gas or a fluid flow through these microchannels. As these electronic components become smaller and smaller [1] and produce relatively more power, new models for temperature and heat flux predictions are necessary.

Conventional approaches used to study heat flow are ranging from continuum to molecular techniques. Continuum represented by the Navier Stokes equations breaks down when the size of these devices decreases or when the flow becomes more dilute [2,3]. The governing equation of the heat flow is then changing from Navier Stokes to Boltzmann equation. This equation involves molecular velocities instead of macroscopic properties. Solving this equation is very difficult since the number of independent variables contains both those of velocity and of physical space. The alternative is to use particle simulation methods to study heat transfer in micro- or nanochannels, like Direct Simulation Monte Carlo (DSMC) [2] or molecular dynamics (MD) [4].

In all these approaches, reliable models of the gas-solid interface are essential for accurate heat flux predictions. Boundary conditions are usually used to represent the gas-solid interface [5–8]. These boundary conditions are crucial for correct heat predictions as the transport properties of gases at the gas-solid interface can play a very important role in the overall behavior in the channel. A lot of effort has been concentrated on studying the gas-surface interface in micro- or nanochannels. In most cases of these analyses, a simplified boundary condition for reflected molecules at a solid surface has been used. This boundary condition called diffuse reflection assumes that the reflected molecules are completely accommodated with the wall surface and their

*s.v.nedea@tue.nl

velocity distribution is given by the Maxwellian distribution with the wall quantities. However, when the molecules have high energy, the diffuse reflection is not applicable, and the scattered flux shows preferred directions (e.g., specular ray direction) [9,10].

Other Maxwell-type boundary conditions are based on the assumption that a fraction $(1-\alpha)$ of molecules is reflected specular from the surface, while α is reemitted diffusely with Maxwell distribution at wall conditions. This α is called the accommodation coefficient and is computed based on the tangential momentum or on the energy of the molecules according to the flow situation [11]. A more elaborated model was proposed by Cercignani and Lampis [5] and developed by Lord [7], and includes two parameters: coefficient of the tangential momentum accommodation parallel to the surface and of energy accommodation normal to the surface.

An alternative to using boundary conditions is to use explicit MD simulations, allowing for the simulation of both walls, gas, and wall-gas interactions explicitly. The interaction of monoatomic gas molecules with solid molecules by using MD was studied by Wachman *et al.* [8], and Matsui and Matsumoto [12]. They computed the behavior of reflection or adsorption of the incident gas molecules, while Yamanishi *et al.* [13] constructed a gas-surface interaction model by developing a multistage collision between molecules based on the analysis of MD. Various other MD studies have been reported for specific gas-solid and fluid-solid interfaces [14,15].

To study the impact on the heat fluxes of gas-surface interactions in realistic channels (microchannels) using explicit MD simulations is however computationally very expensive. The idea is to combine MD and Monte Carlo (MC) to cover larger time and length scales. Hybrid methods are such techniques used to study the gas-surface interface using molecular dynamics techniques and the flow region with MC. These techniques are very accurate, but to simulate the MD region taking into account explicitly the walls and the fluid in the surface vicinity region is still computationally very demanding. Previously, we have introduced a hybrid simulation approach combining MD and MC simulations to study dense and dilute gas in nanochannels [16]. Yamamoto *et al.* [11] used another hybrid approach combining MD and DSMC for the motion of molecules between two walls and investigating the characteristics of the reflected nitrogen gas molecules at a platinum surface [11,17]. Based on their results on the observed trajectories of gas molecules, the gas molecules bounce on the surface (once, twice, or many times), and eventually return. In some cases, the molecules are adsorbed on the surface, and leave after a while. From the trajectories they could not deduce that the Maxwell-type distribution function consisting of the specular and diffuse reflections describes well the distribution function of the reflected molecules. However, the global velocity is well described by this distribution if the accommodation coefficient involved is properly chosen.

Based on this result, we investigate the gas-surface interface for a gas between two parallel walls [18] and we compute the accommodation coefficients α based on explicit MD simulations. We compute α by averaging over individual trajectories of molecules impinging and reflecting from the explicit wall in an MD simulation. Based on these molecular fluxes we compute α from the temperature distribution between the walls (${\alpha_T}^{\mathrm{MD}}$), from the heat fluxes of the corresponding impinging and reflecting molecular fluxes ($\alpha_{qx}^{\mathrm{MD}}$), and also from the total average heat flux between the walls (${\alpha_{q_x}}_{\mathrm{avg}}^{\mathrm{MD}}$). First, these α coefficients are computed for a dilute gas using MD with explicit wall boundary conditions and different gas-wall interactions (attractive, repulsive). These accommodation coefficients are introduced into an MC simulation based on Maxwell-type boundary conditions. The technique of computing these accommodation coefficients based on temperature was already given in [19]. In this paper we compute α not only from the temperature, but also from the heat flux and from the average heat flux in the system. Moreover, in [19] an average of the α computed next to the cold and warm wall is given (${\alpha_T}^{\mathrm{MD}}$), while here the α coefficients are computed separately next to the cold and warm wall (i.e., ${\alpha_T}_c^{\mathrm{MD}}$ and ${\alpha_T}_w^{\mathrm{MD}}$). These α's that give good results for the total heat flux in the system are validated. It is also checked to retrieve the α's used as input from MD back from the MC simulations both near the warm and near the cold wall. The effect of the diffusive-specular Maxwell-like boundary conditions using these α coefficients on different properties is analyzed. The properties considered are the temperature, density, and heat flux profiles of the total molecules confined between the two walls, but also on the temperature, density, and heat flux profiles of the incident and reflected molecules near the channel wall. These results are compared with the results of pure MD simulations with explicit wall simulation and with MC results using pure Maxwell boundary conditions ($\alpha = 1$). Building the map of the MC heat flux dependence on a generic α, an effective α is found by confronting these MC heat fluxes (q_c^{MC}) with MD heat fluxes (q_x^{MD}) as also described in [19]. Further, we study for both hydrophilic and hydrophobic gas-wall interactions the effect of different fluid-wall molecular mass and radius ratios on the heat flux predictions in the channel. The results are used to predict the thermal behavior for two different systems: (a) an argon gas interacting with a platinum surface channel; (b) a xenon gas interacting with a platinum surface channel. The values of ${\alpha_T}^{\mathrm{MD}}$ are compared with experimental results of scattering of molecular beams by metallic surfaces in [17,20,21] and with Yamamoto's molecular model in [11,17].

As α is a gas-wall characteristic derived from gas fluxes in the immediate vicinity of the wall, and it does not depend on the Kn number [22], we use the same approach to study heat flux in a micro- or nanochannel for a dense gas. First we transfer the accommodation coefficients computed from the MD simulation of the gas-wall interaction of a dilute gas to an MC simulation based on Enskog equation [23,24] with Maxwell-type boundary conditions, and we compare the heat fluxes computed using these two approaches. The difference with the values of α computed for a dilute gas in [19] is that in this case we report here also the results for the case when gas-gas interactions equal the gas-wall interactions, while in [19] the gas-gas interactions were only modeled as hard-sphere.

A map for the dependence of MC heat fluxes q_x^{MC} on a generic α is given also for a dense gas. The effective α is established by confronting the MD results on heat fluxes q_x^{MD} with the MC results q_x^{MC} given in the map. The values found

for α are more accurate in this case then the ones computed from a dilute gas, as in the case of a dense gas there are no temperature jumps near the wall.

II. MODEL FOR GAS-SURFACE INTERACTIONS

Our model to study the two-dimensional heat flow in a microchannel consists of two parallel plates of length L_y at a distance L_x apart from each other and of gas molecules confined between these two walls. This model was also previously used and described in [19]. Moreover, the simulation setup was described in detail in previous papers [16,18,19,25] and it is given here just for the sake of completeness. Both plates have their own temperature, T_1 and T_2, respectively, where this temperature is uniform on the plate surface and constant in time, and $T_2/T_1 = 0.5$. The gas consists of spherical particles of diameter a and mass m, at temperature T. The density of the gas can be expressed as n, being the number of particles per unit of volume, or using a reduced density η, which also takes the particle sizes into account and is related to the number density as $\eta = \pi n a^3/6$ [24]. The mean free path of the gas particles is related to this reduced density. For a relatively dense gas with $\eta = 0.1$, the mean free path $\lambda = 1/\sqrt{2}\pi a^3 n Y(\eta)$ and the molecular diameter a have the same order of magnitude. The $Y(\eta)$ factor is the pair correlation function at contact [23,24]. The distance L_x between the plates, in the x direction, is always such that both plates are only a few mean free paths apart. The walls can be modeled explicitly (based on an MD model) or using boundary conditions (Maxwell or Maxwell-like boundary conditions in an MC or MD model). Two situations were considered: (a) a dilute gas confined between the walls with the reduced density $\eta = 0.005$, $L_x = 1.39\lambda = 32a$, $L_y = 2.03\lambda = 46.73a$, and (b) a dense gas with $\eta = 0.2$ and $L_x = 95\lambda = 31.93a$, $L_y = 139.49\lambda = 46.90a$. The number of bins in the x direction is $N_{\text{cells}} = 100$ and the volume of one bin being $d_x L_y L_z$ with $d_x = L_x/N_{\text{cells}}$. In MD, a Lennard-Jones (LJ) potential [4] is used to model the interactions between the gas-gas, gas-wall, and wall-wall molecules [18]. A truncated shifted Lennard Jones (tsLJ) potential [4] is used to keep only the repulsive contribution as a model for purely repulsive molecules. Here the tsLJ potential has the form

$$V_{\text{tsLJ}} = \begin{cases} V_{\text{LJ}}(r) - V_{\text{LJ}}(r_c) & \text{if} \quad r \leqslant r_c, \\ 0 & \text{if} \quad r > r_c, \end{cases} \tag{1}$$

where r_c is the cutoff radius and V_{LJ} is the Lennard-Jones potential:

$$V_{\text{LJ}}(r) = \epsilon \left[\left(\frac{2R_{\text{vdW}}}{r} \right)^{12} - 2 \left(\frac{2R_{\text{vdW}}}{r} \right)^{6} \right]. \tag{2}$$

The geometry is given for the sake of completeness in Fig. 1(b). The real geometry contains also the second gas chamber in order to balance the collisions which on both sides will cancel out. The two walls consisting of 18 000 particles each forming a face centered cubic (fcc) lattice are placed in a box of size $95.0\lambda \times 139.49\lambda \times 139.49\lambda$ in case $\eta = 0.2$, and in a box of size $1.39\lambda \times 2.03\lambda \times 2.03\lambda$ in case of $\eta = 0.005$, and are separated from each other in x direction. The total number of gas molecules in the box is 55 998 for $\eta = 0.2$ and 1300 corresponding for $\eta = 0.005$. The walls are formed in previous simulations by randomly placing the particles in the simulation box and cooling the system down until crystallization occurs. The six atom layers were not restricted in any way, such that the walls can in principle move through the simulation box. However, the mass of the wall is large compared to the mass of one gas particle such that a single collision hardly affects the wall. Moreover, for this geometry, forces exerted on the wall from both sides cancel each other. The temperature of the two walls can be controlled independently by coupling them to a heat bath, whereas the gas can only heat up or cool down by collisions with the walls. More details on the setup of the molecular simulations are explained in [16,18]. Reduced units are used in all simulations presented and these units are here described. The reduced units used in our MD model are the unit of length (σ^*), the unit of mass (m^*), and the unit of energy (ϵ^*). All other units can be derived out of these choices [16,18]. The mass and the size of the wall particles are taken here as unity: $m^* = 195$ g/mol, $\epsilon^*/k_B = 628.58$ K, and $\sigma^* = 2.523$ Å. Based on these units, the temperatures of the two walls are $T_1 = 1.0[\epsilon^*/k_B] = 628.5$ K and $T_2 =$

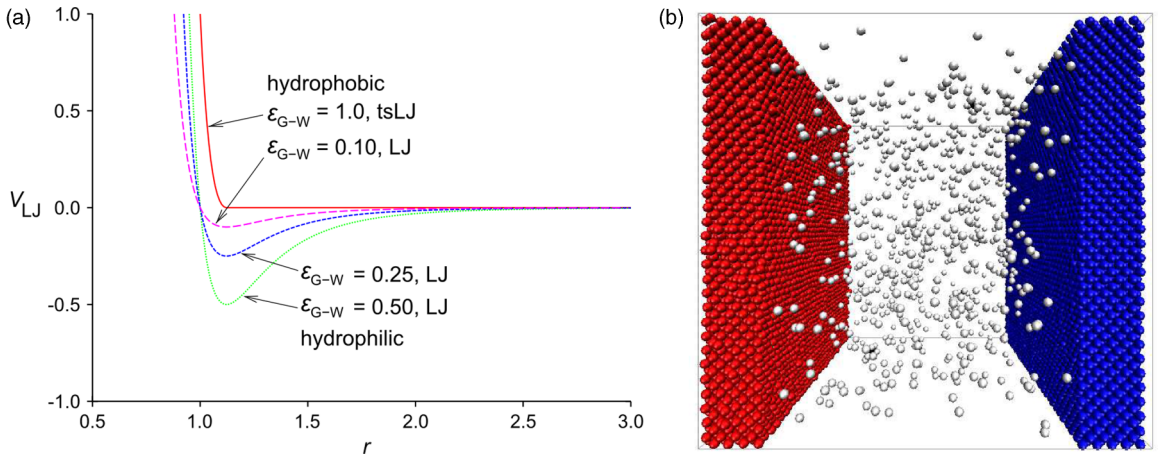

FIG. 1. (Color online) (a) Lennard Jones (LJ) potential for $\epsilon_{G\text{-}W} = 0.1, 0.25, 0.5$ and truncated shifted Lennard Jones potential (tsLJ) for $\epsilon_{G\text{-}W} = 1.0$; (b) geometry of the MD simulation domain (left = warm wall; right = cold wall; middle = gas molecules in between).

$0.5[\epsilon^*/k_B] = 314.25$ K. The walls are kept together by a strong interaction strength $\epsilon_{W\text{-}W} = 6.0$ in the LJ potential. The gas-wall interactions can be hydrophilic (attractive) or hydrophobic (repulsive) wall interactions. The definition for the two potentials used to model hydrophilic and hydrophobic wall interactions was also given in [19]. Attractive gas-wall interactions are modeled here as well by LJ with $\epsilon_{G\text{-}W}$ between 0.25 and 0.50, and repulsive wall interactions by tsLJ with $\epsilon_{G\text{-}W} = 1.0$, or by LJ with a very small $\epsilon_{G\text{-}W}$ (e.g., $\epsilon_{G\text{-}W} = 0.1$). As shown in [19], the shape of the Lennard-Jones potential for different interaction strengths has the form in Fig. 1(a).

From MD simulations, macroscopic properties can be derived. The heat fluxes are computed here using the relation

$$\vec{q} = \frac{d}{dt}\sum_i \vec{r}_i E_i, \tag{3}$$

where $\vec{r}_i$ is the position and E_i is the energy associated with particle i. The kinetic and potential parts of the heat fluxes are

$$\vec{q}_{\text{kin}} = \sum_i E_i^{\text{kin}}\vec{v}_i = \frac{1}{2}\sum_i m_i v_i^2 \vec{v}_i, \tag{4}$$

$$\vec{q}_{\text{pot}} = \frac{1}{2}\sum_{i,j}(\vec{F}_{ij}\cdot\vec{v}_i)\vec{r}_{ij} + \sum_i E_i^{\text{pot}}\vec{v}_i, \tag{5}$$

where m_i and $\vec{v}_i$ are respectively the mass and the velocity of particle i, and $\vec{F}_{ij}$ and $\vec{r}_{ij}$ are the interaction force and separation vector between particle i and j.

These fluxes were computed in the defined $N_{\text{cells}} = 100$ bins, having the volume equal to $dx\,L_y L_z$, where $dx = L_x/N_{\text{cells}}$.

III. EFFECTIVE ACCOMMODATION COEFFICIENTS FOR A DILUTE GAS FROM TEMPERATURE OF THE INCIDENT AND REFLECTED MOLECULAR FLUXES

In our previous work [18], we used a MD approach to study the wettability effect on heat and particle flow in nanochannels. The results on the heat flux predictions in a channel where particles are sticking to the wall (attractive wall interactions) were given, showing that the relevant parameter is the gas-wall interaction strength, whereas gas-gas interaction is of much less importance on the resulting heat flux.

In [18] we have seen that, at low densities, density peaks depending on the attractive gas-wall interaction potential are present and that this effect is reflected in increased gradients in the temperature near the wall interface. As a result of particles sticking to the wall, their velocity is adapted much more to the wall temperature, such that the higher the attraction, the higher the difference in temperature between gas particles going to the left (incident) and particles moving to the right (reflected). Simulations have been done in order to understand these effects [19]. We use MD with explicit wall interactions to get the temperature and density profiles of the particles moving from the cold to the warm wall (C-W), from the warm to the cold wall (W-C), and the profiles of the total temperature and densities, as these properties are changing with the gas-wall interactions.

In [19] we reported the results for the temperature of the molecular fluxes impinging and reflected from the surface.

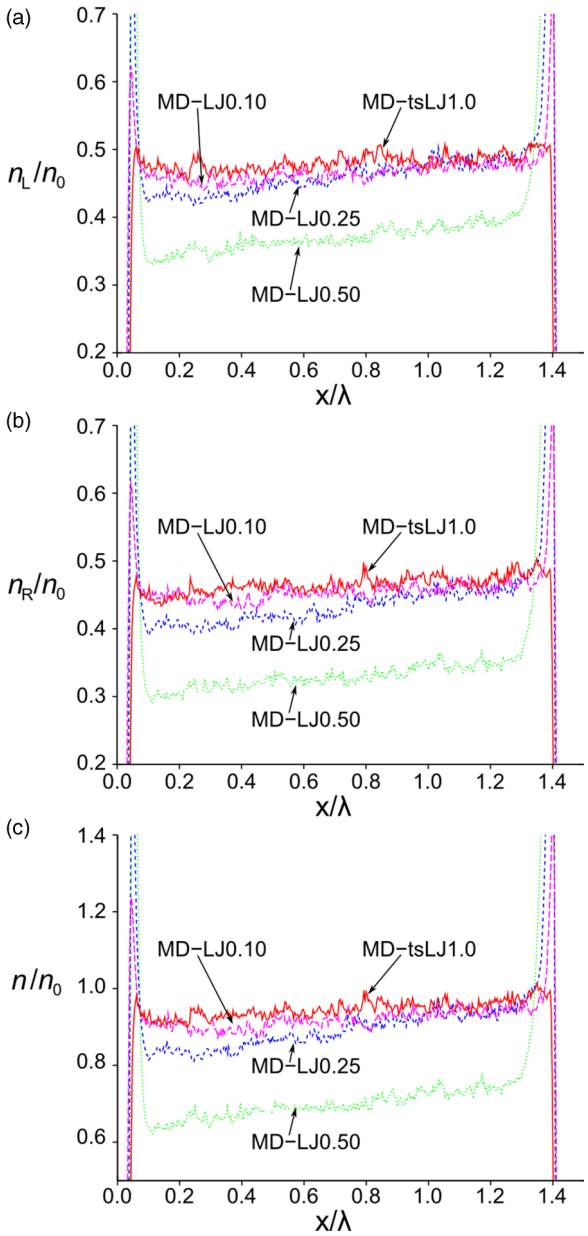

FIG. 2. (Color online) (a) MD number density of particles going to the left wall (cold-warm). (b) MD number density of particles going to the right wall (warm-cold). (c) MD total number density of particles between the walls. All the quantities are normalized with reference density $n_0 = 0.01$ and $\eta = 0.005$.

Here we look also at the density distribution of the molecular fluxes. In Figs. 2 and 3, we see that there are more particles going from the C to the W wall, than from the W to the C wall for more attractive walls (hydrophilic), and they are almost equal for repulsive wall interactions (hydrophobic). The slope of these profiles are varying with the gas-surface interaction strength, $\epsilon_{G\text{-}W}$, and peaks are present in the temperature and density profiles when increasing $\epsilon_{G\text{-}W}$. The high density peaks correspond to the layer of particles adsorbed or sticking to the wall and higher peaks determine increased α also reflected in the T slopes. The higher the slope in T next to the wall, the higher the thermall accommodation at the wall. The effective

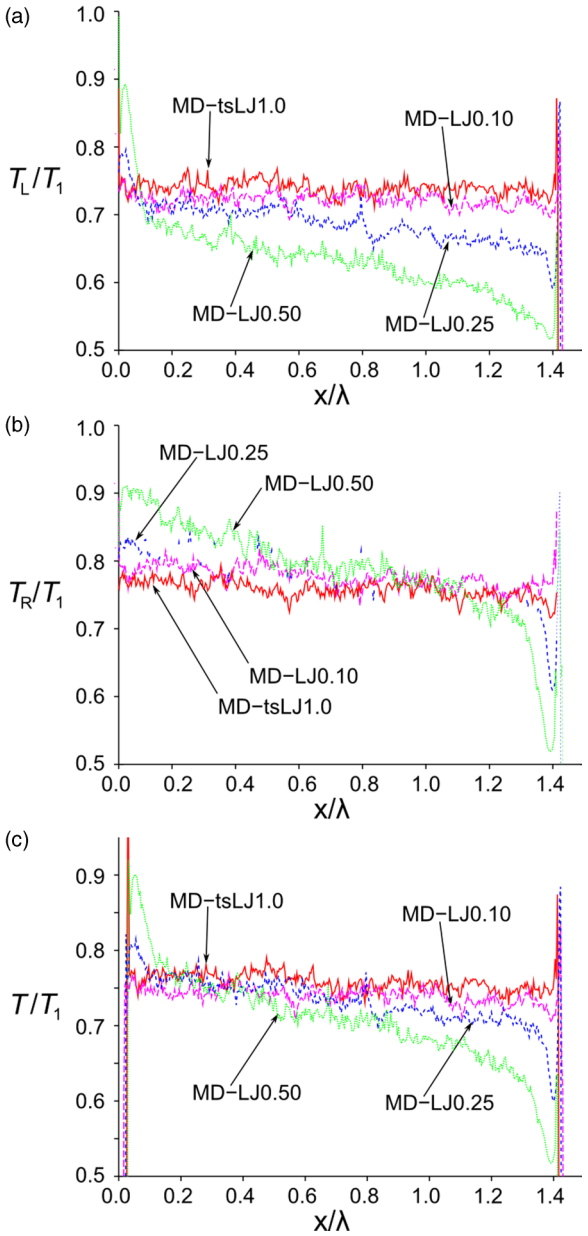

FIG. 3. (Color online) (a) MD results for the temperature of particles going to the left wall (cold-warm). (b) MD results for the temperature of particles going to the right wall (warm-cold). (c) MD results for the total temperature of particles between the walls. All the quantities are normalized with the temperature of the warm wall T_1 and $\eta = 0.005$.

accommodation coefficient α can be computed based on the temperature of the incident and reflected molecules in the immediate vicinity of the wall like it was computed also in [19].

From all these MD simulations for hydrophilic and hydrophobic wall interactions, we extract the accommodation coefficients based on the temperature, energy, and average energy of the impinging and reflected molecular fluxes. In [19] only the accommodation coefficients based on temperature were computed and averaged near the warm and the cold wall. Now we compute these coefficients from the other properties

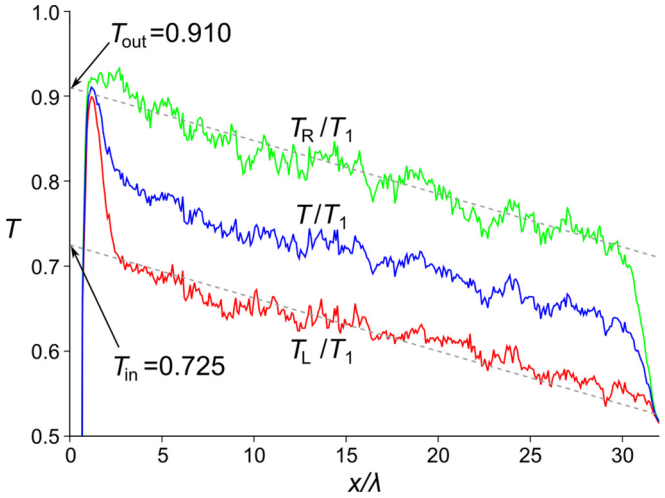

FIG. 4. (Color online) Temperature profiles of the impinging (T_{in}), reflected (T_{out}), and total molecules (T) for a channel having $n_0 = 0.01$, $\eta = 0.005$, and the gas-surface interactions are characterized by $\epsilon_{G\text{-}W} = 0.5$. From the temperatures near the warm wall, T_{in} and T_{out}, and surface temperature T_S, the accommodation coefficient $\alpha_{T_w}^{MD}$ is computed.

both next to the warm and cold wall and we compare the influence on the heat flux predictions using these separate values.

The effective accommodation coefficient based on T has the form

$$\alpha_T = (T_{in} - T_{out})/(T_{in} - T_S),$$

where T_{in} is the temperature of the particles moving towards the wall (incident), T_{out} is the temperature of particles leaving from the wall (reflected), and T_S is the temperature of the considered wall surface. Using the definition, we compute all the α_T's from the MD temperature profiles for different G-W interactions (attractive: LJ $\epsilon_{G\text{-}W} = 0.10, 0.25, 0.5$; repulsive: tsLJ $\epsilon_{G\text{-}W} = 1.0$). The values for T_{in} and T_{out} for a given system are taken as shown in Fig. 4.

In Fig. 4 we show the MD temperature profiles between the explicit walls for a dilute gas with $\eta = 0.005$ and $\epsilon_{G\text{-}W} = 0.5$. In this case the accommodation coefficient α_T is 0.67, when the gas molecules have the same mass as the wall molecules. The temperature of the gas to the wall is taken by extending the average bulk temperature as shown in the figure. This method to compute α near the wall was explained in detail in [19] and it is based on computing the best linear fit through the MD points for both T_L and T_R (the linear fit is corresponding to the continuous lines in Fig. 4). The values of T_{in} and T_{out} correspond to the points where these linear fittings for T_L and T_R reach the wall. As the walls are not restricted in any way in the simulations, we used exactly the position of the wall density peaks to determine these exact points.

In the same way we compute α for each $\epsilon_{G\text{-}W}$ from all the MD temperature profiles. This can be seen also in Table I, where the last two columns indicate the accommodation coefficient α computed from the MD temperature profiles as previously described, next to the warm and also next to the cold wall. The values of the accommodation coefficient

TABLE I. Accommodation coefficient α computed from MD for different values of $\epsilon_{G\text{-}W}$ in the gas-wall interaction potential (Lennard-Jones) shown in column 1. These values are given as input in MC with Maxwell-like boundary conditions. The MC values of α near the warm wall corresponds with the values of α computed from MD temperature profiles and given as input in the MC simulations. A dilute gas was considered with $\eta = 0.005$.

$\epsilon_{G\text{-}W}$	MC α_{T_w}	MC α_{T_c}	MD α_{T_w}	MD α_{T_c}
tsLJ 1.0	0.15	0.15	0.15	0.14
LJ 0.10	0.15	0.15	0.16	0.17
LJ 0.25	0.40	0.44	0.37	0.41
LJ 0.50	0.70	0.76	0.67	0.74

α_T are similar for hydrophobic gas-wall interactions (small values of $\epsilon_{G\text{-}W}$), but very different for hydrophilic gas-wall interactions (when $\epsilon_{G\text{-}W}$ increases). The value of α_T computed next to the warm wall is used in the Maxwell-like boundary conditions in MC simulations such that only a fraction α_T from the impinging molecules is thermalized by the wall. This input value of ${\alpha_T}^{\mathrm{MD}}$, computed from MD, is checked to be retrieved from the resulting MC temperature profiles. From the first two columns after $\epsilon_{G\text{-}W}$ of Table I, we see that the MD values of ${\alpha_T}^{\mathrm{MD}}$ both near the warm and cold wall considered as input for the Maxwell-like boundary in MC are retrieved from the MC temperature profiles for all the considered interactions (columns 2 and 3).

We compute now α based on the heat fluxes: from the heat fluxes of impinging and reflected molecules,

$$\alpha_{q_x} = \left(q_{x_{\mathrm{in}}} - q_{x_{\mathrm{out}}}\right)/\left(q_{x_{\mathrm{in}}} - q_{x_{\mathrm{out(Max)}}}\right),$$

and also from the average total heat fluxes,

$$\alpha_{q_{x\,\mathrm{avg}}} = q_x/q_{x\mathrm{Max}} = \left(q_{x_{\mathrm{in}}} + q_{x_{\mathrm{out}}}\right)/q_{x\mathrm{Max}}.$$

In the expression for the α_{q_x} accommodation coefficient, $q_{x_{\mathrm{in}}}$ is the heat flux of all the particles moving to the left (impinging flux), $q_{x_{\mathrm{out}}}$ is the heat flux of particles going to the right (reflected), and $q_{x_{\mathrm{out(Max)}}}$ is the heat flux of particles going to the right (reflected) when there are Maxwell B.C. The $\alpha_{q_{x\,\mathrm{avg}}}$ values are computed by taking the ratio between the total heat flux (q_x) (see Fig. 5), which is the sum of the impinging and reflected molecular heat fluxes, and the total heat flux using Maxwell B.C.

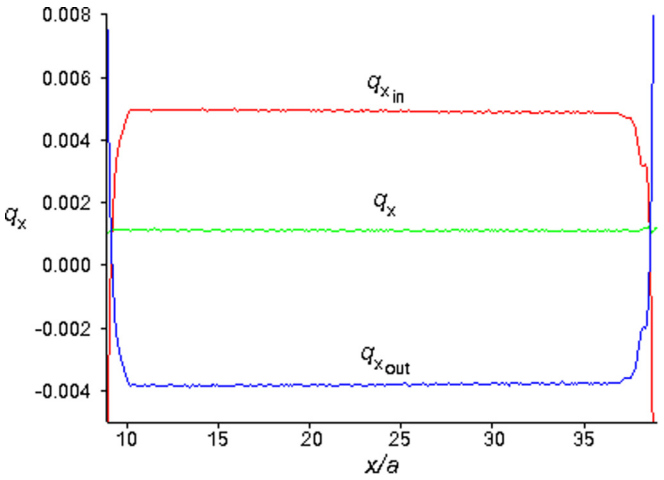

FIG. 5. (Color online) Heat flux profiles of the impinging ($q_{x_{\mathrm{in}}}$), reflected ($q_{x_{\mathrm{out}}}$), and total heat fluxes ($q_{x\,\mathrm{avg}}$) for a channel having $n_0 = 0.01$, $\eta = 0.005$, and the gas-surface interactions are characterized by $\epsilon_{G\text{-}W} = 0.5$. From the heat flux value near the warm wall, $q_{x_{\mathrm{in}}}$ and $q_{x_{\mathrm{out}}}$, and surface temperature $q_{x_{\mathrm{out(Max)}}}$, the accommodation coefficient ${\alpha_{q_x}}^{\mathrm{MD}}$ is computed.

In Table II we compare also the heat flux predictions from pure MD simulations with explicit gas-wall interactions and the heat fluxes from MD with Maxwell boundary conditions, and we show the corresponding heat fluxes associated to the impinging and reflected fluxes of molecules (fluxes of particles moving towards the cold and the warm wall). As expected, there are large deviations for all the values of the gas-wall interactions between MD heat predictions with explicit walls and MD predictions with Maxwell B.C. The columns 3, 4, and 5 of Table II are going to be used to compute the accommodation coefficients $\alpha_{q_{x\,\mathrm{avg}}}$ and α_{q_x} based on the total heat fluxes and on the heat flux profiles of the impinging and reflected molecular fluxes. In Table III, we compare them with α_T computed from the temperature profiles of these molecular fluxes. As the errors for α_c are similar with α_w, we focus on analysis near one wall (warm wall).

In Table III we find the results of all these accommodation coefficients α, computed based on temperature (α_T), average heat fluxes ($\alpha_{q_{x\,\mathrm{avg}}}$), or heat fluxes next to the warm wall ($\alpha_{q_{x_w}}$). All these α's are used as input for MC simulations with α dependent Maxwell B.C. The heat flux predictions

TABLE II. Heat fluxes using explicit MD with different $\epsilon_{G\text{-}W}$ (column 2) and with pure Maxwell boundary conditions, and also MC heat fluxes computed using Maxwell-like B.C. based on different α (see Table III). Column 2: the gas-wall interaction strength for the LJ potential; column 3: the total MD heat fluxes; column 4: heat flux of impinging molecules going to the left; column 5: heat flux of reflected molecules going to the right. The MC heat flux values in column 6 are computed based on the α computed from the temperature profiles (α_T), in column 7 from the total heat fluxes ($\alpha_{q_{x\,\mathrm{avg}}}$), and in column 8 from the heat flux profiles computed near the warm wall ($\alpha_{q_{x_w}}$). A dilute gas was considered with $\eta = 0.005$.

Explicit	$\epsilon_{G\text{-}W}$	${q_x}^{\mathrm{MD}}$	${q_{x_{\mathrm{in}_w}}}^{\mathrm{MD}}$	${q_{x_{\mathrm{out}_w}}}^{\mathrm{MD}}$	${q_x}_T^{\mathrm{MC}}$	${q_{x\,\mathrm{avg}}}^{\mathrm{MC}}$	${q_x}_w^{\mathrm{MC}}$
	tsLJ 1.0	0.000 50	−0.0047	0.0052	0.000 22	0.000 36	0.000 50
	LJ 0.10	0.000 50	−0.0044	0.0049	0.000 22	0.000 36	0.000 50
	LJ 0.25	0.000 84	−0.0041	0.0049	0.000 72	0.000 90	0.000 84
	LJ 0.50	0.00114	−0.0028	0.0040	0.001 31	0.001 31	0.001 31
Max. B.C.		0.0021	−0.0036	0.0057			

TABLE III. Accommodation coefficients computed for each gas-wall interaction parameter in column 1 from the MD temperature profiles (column 2), average MD heat flux profiles, and local average heat fluxes next to the warm wall. A dilute gas was considered with $\eta = 0.005$.

$\epsilon_{G\text{-}W}$	α_T	$\alpha_{q_{x\,\mathrm{avg}}}$	$\alpha_{q_{x\,w}}$
tsLJ 1.0	0.15	0.21	0.30
LJ 0.10	0.15	0.21	0.30
LJ 0.25	0.40	0.40	0.50
LJ 0.50	0.70	0.70	0.70

from these MC simulations (columns 6, 7, and 8 in Table II) are compared to pure MD simulations with explicit wall interactions (columns 3, 4, and 5 in Table II). In these simulations, the gas-gas interactions are considered equal to the gas-wall interactions. From these results we can validate the α's that give good results for the heat flux predictions when used in the B.C. for MC simulations. We find that $\alpha_{q_{x\,\mathrm{avg}}}$ obtained from the average heat fluxes ($q_{x_{\mathrm{avg}}}$) and from the heat fluxes of impinging and reflected molecules α_{q_x} give good results for the q_x predictions when compared to results from explicit MD simulations for both hydrophilic and hydrophobic wall interactions, while α_T gives good results for hydrophilic but not for hydrophobic wall interactions (see Table II).

Until now we have seen how these α's influence the average quantities of the molecular fluxes. Further we analyze how the profiles of the total density, total temperature, and density and temperature of the impinging particles (moving towards the wall) and reflected particles (moving away from the wall) are changing with the wall properties. For this, we compute all these properties using different B.C.: Maxwell (thermal wall B.C.), Maxwell-type based on α, and explicit MD simulations. Here we give and compare the results for two interaction strengths for both the temperature and density profiles. For more interaction strengths, the temperature profiles were shown in detail in [19].

In Fig. 6 we compare the density and temperature profiles for all the molecules of a dilute gas using explicit MD simulations for the boundary conditions, and also Maxwell and Maxwell-like boundary conditions based on α_T. We notice that both for hydrophilic and for hydrophobic walls, the results for the Maxwell-like B.C. give different results when compared with explicit MD simulations both for hydrophilic and hydrophobic wall interactions.

In Fig. 7, we compare density and temperature profiles for the impinging and reflected molecular fluxes, using again explicit MD, Maxwell, and Maxwell-like B.C. based on α for hydrophilic and hydrophobic wall interactions. Comparing the density profiles, we see that the number of molecules going from the warm to the cold wall is much smaller than the number of molecules going from the cold to the warm wall in the case of hydrophilic wall interactions ($\epsilon = 0.25, 0.5$), and they become equal for lower ϵ (hydrophobic wall interactions). Also, the higher the ϵ, the better the agreement with Maxwell prediction with full accommodation. The same effect can be seen also on the T profiles: for hydrophobic wall interactions, the temperature of the impinging and reflected molecules are very

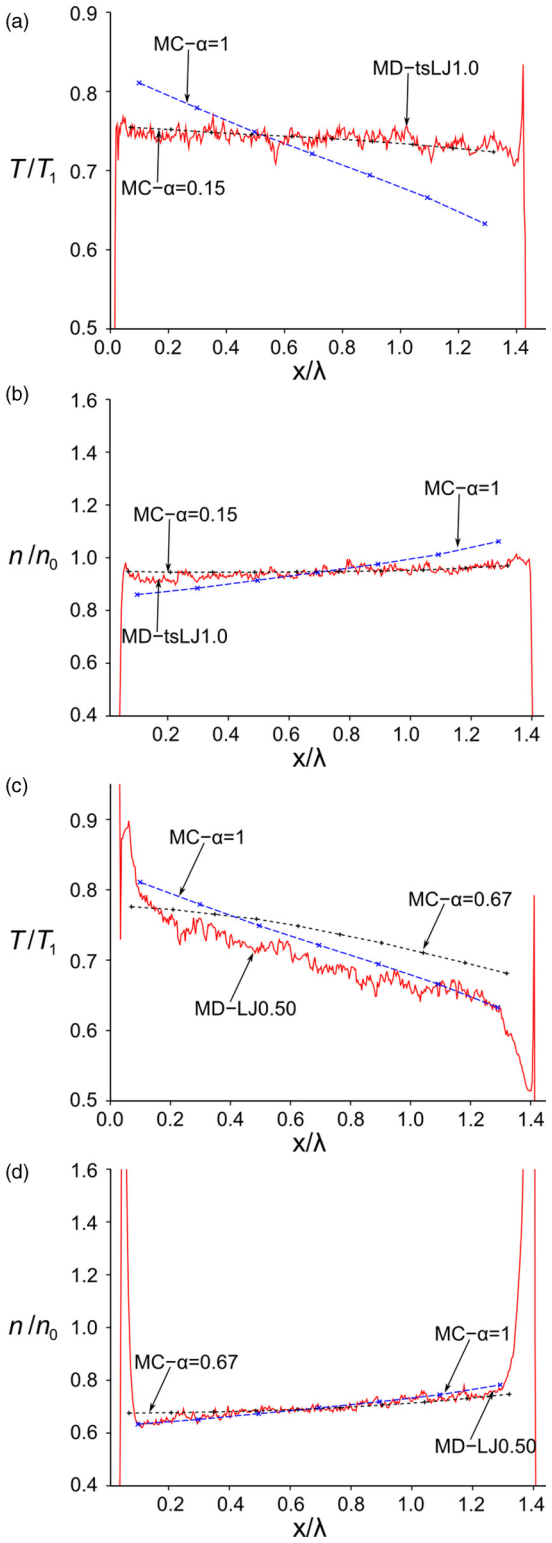

FIG. 6. (Color online) Density and temperature profiles of the total particles between the two walls. The parameters for the MD and MC simulations are (a) and (b) hydrophobic interactions: MC with Maxwell-like B.C. including $\alpha_T{}_w^{\mathrm{MD}} = 0.15$; MC with pure Maxwell B.C. with $\alpha = 1.0$; MD: $\epsilon_{\mathrm{tsLJ}} = 1.0$; (c) and (d) hydrophilic interactions: MC with Maxwell-like B.C. including $\alpha_T{}_w^{\mathrm{MD}} = 0.67$; MC with pure Maxwell B.C. with $\alpha = 1.0$; MD: $\epsilon_{\mathrm{LJ}} = 0.50$. The densities are normalized with $n_0 = 0.01$, and the temperatures are normalized with $T_0 = T_1$ (warm wall temperature) and $\eta = 0.005$.

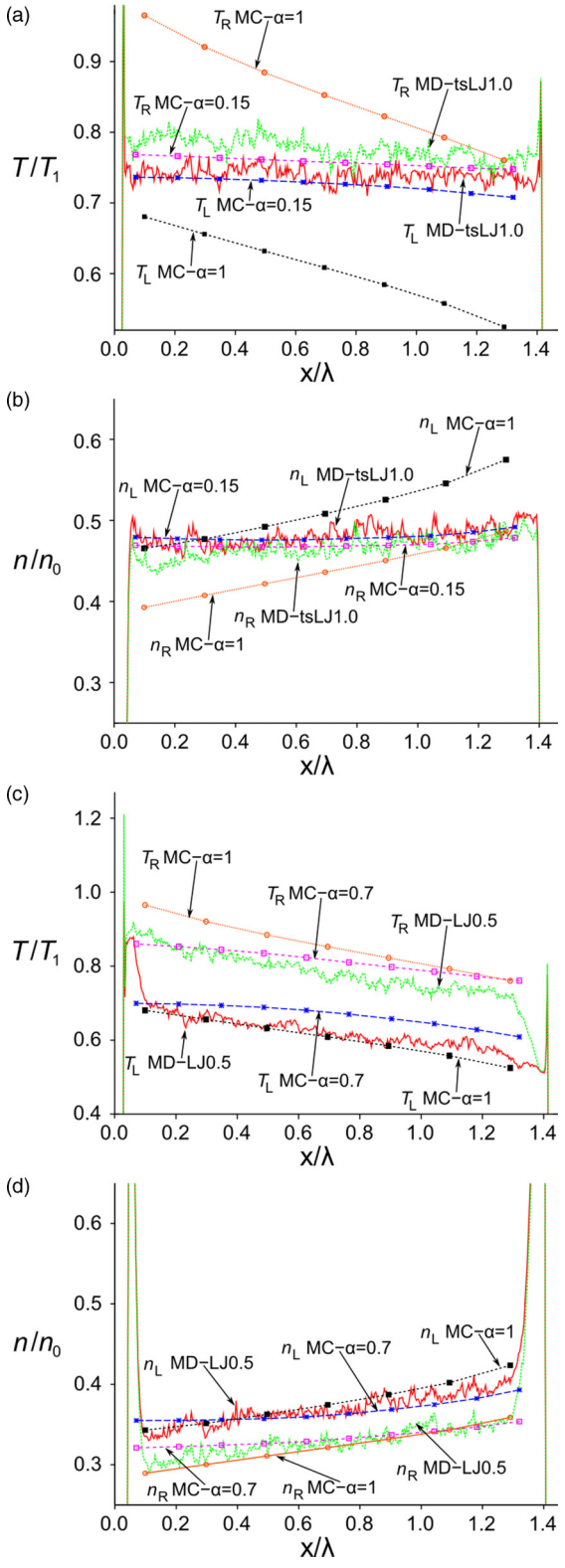

FIG. 7. (Color online) Profiles for the temperature and number of particles going to the left wall (cold-warm) and to the right wall using MD and MC. The parameters for the MD and MC simulations are (a) and (b) hydrophobic: MC: $\alpha_{Tw} = 0.15$; MC: $\alpha = 1.0$; MD: $\epsilon_{\text{tsLJ}} = 1.0$; (c) and (d) hydrophilic: MC: $\alpha_{Tw} = 0.70$; MC: $\alpha = 1.0$; MD: $\epsilon_{\text{LJ}} = 0.50$. All the quantities are normalized with $n_0 = 0.01$ and $\eta = 0.005$.

close to each other, while for hydrophilic wall interactions, temperature of impinging molecules is much lower than the temperature of the reflected molecules and the agreement with Maxwell B.C. ($\alpha = 1$) is better.

This effect was quantified in [19] showing the influence of different interaction strengths on the average temperature and average density of the impinging and reflected molecular fluxes between the cold and the warm wall. When comparing the average measurements for explicit MD B.C. and Maxwell-like B.C. based on α, we could see also that averaged density and temperature of incident and reflected molecules correspond very well for hydrophobic interaction (low ϵ), while for hydrophilic interactions, the clustering next to the wall becomes important and large differences between the molecular fluxes and their temperature are registered. From these results we can conclude that when concerning reproducing the molecular fluxes between the two walls, MC is able to predict this very well for the hydrophobic interactions where the peaks in the profiles are absent near the boundaries. Also, the accommodation coefficient α_{q_x} gives good predictions for the total heat flux in the system.

IV. USING THE EFFECTIVE ACCOMMODATION COEFFICIENT FOR THE HEAT FLUX PREDICTIONS FOR A DENSE GAS

As the accommodation coefficient describes the energy transfer in the gas-surface interface, we transfer these coefficients computed from MD for a dilute gas to study the heat fluxes for a dense gas confined between the walls of a micro- or nanochannel.

In [19] we determined the heat flux q_x in a channel with wall separation $L_x = 95\lambda$ and $\eta = 0.2$, for different wall-gas and gas-gas interactions. We give the results for the explicit simulations also here as they are going to be used to compute all the accommodation coefficients based on heat fluxes for a dense gas. We would also like to emphasize again that the results in Table IV show that the gas-gas interactions become important, such that the higher the $\epsilon_{G\text{-}G}$, the lower the heat flux. When walls are very attractive, then the role of gas-gas interactions becomes less important. This is different from the dilute gas simulations when the gas-gas interactions had no impact on the heat fluxes.

Pure diffusive thermal walls (Maxwell B.C.) overestimate the MD heat fluxes for both hydrophilic and hydrophobic wall interactions. When using the α_{q_x}'s computed from the

TABLE IV. Heat flux using MD with different wall-gas and gas-gas LJ interaction potential, for a dense gas with $\eta = 0.2$. The columns stand for the wall-gas interactions and the rows for the gas-gas interactions.

q_x		$\epsilon_{G\text{-}W}$			
		tsLJ 1.0	LJ 0.10	LJ 0.25	LJ 0.50
$\epsilon_{G\text{-}G}$	tsLJ 1.0	0.015	0.014	0.016	0.017
	LJ 0.10	0.012	0.010	0.014	0.015
	LJ 0.25	0.012	0.011	0.013	0.016
	LJ 0.50	0.009	0.009	0.012	0.016

TABLE V. Heat fluxes using MD and MC with Maxwell-like boundary conditions based on the accommodation coefficient α for a dense gas with $\eta = 0.2$ and $L_x = 95\lambda$. Column 1 contains the gas-wall interaction strength for the LJ potential, column 2 the accommodation coefficient computed from the heat flux profiles of a dilute gas for each G-W interaction, column 3 the MC heat predictions, columns 4 and 5 the MD heat flux predictions for the case of $\epsilon_{G\text{-}G=\text{tsLJ}} = 1.0$ and $\epsilon_{G\text{-}G} = \epsilon_{G\text{-}W}$, and columns 6 and 7 are the deviations of the MD results from the MC ones for these two cases.

G-W	α_{q_x}	q_x^{MC}	tsLJ ($\epsilon_{G\text{-}G} = 1.0$) q_x	($\epsilon_{G\text{-}G} = \epsilon_{G\text{-}W}$) q_x	dev_1	dev_2
tsLJ 1.0	0.21	0.0123	0.015	0.015	0.18	0.18
LJ 0.10	0.21	0.0123	0.014	0.011	0.12	0.11
LJ 0.25	0.40	0.0174	0.016	0.014	0.08	0.24
LJ 0.50	0.70	0.0203	0.017	0.016	0.19	0.26
Maxwell	1.0	0.021				

gas-surface interface of a dilute gas in the Maxwell-like B.C. for a dense gas ($\eta = 0.2$), we find (comparing with MD heat predictions) that the heat fluxes q_x compare good for hydrophobic, but not for hydrophilic wall interactions due to the overlapping effects of attractive and clustering boundary (see Table V). The results of comparisons for the heat fluxes using α_T can be found in [19].

In Table V we consider two situations for the gas-gas interactions: (1) fixed purely repulsive gas-gas interactions for all the gas-wall interactions considered and (2) varying gas-gas interactions such that the gas-gas interactions are equal to the gas-wall interactions. In this way we can compare the effect of different gas-gas interactions on the total heat flux q_x by varying them from hydrophilic to hydrophobic gas-gas interactions and considering the competing effect between the gas-gas and gas-wall interactions. The choice for hard repulsive gas-gas interactions comes also natural to be considered in MD as the q_x values are compared with results of the MC model based on the Enskog equation assuming hard-sphere gas-gas interactions. Columns 6 and 7 of Table V contain the deviations of the MC results with Maxwell B.C. based on α (imported from dilute gas temperature profiles) from the explicit MD heat fluxes. These deviations are given for the two situations of the gas-gas interactions already mentioned (dev_1 and dev_2) and for all the gas-wall interaction strengths considered. The deviations of the MC heat flux q_x with Maxwell B.C. based on α_T from the explicit MD heat fluxes is $dev = [{q_x}^{\text{MD}} - {q_x}^{\text{MC}}(\alpha_T)]/{q_x}^{\text{MD}}$. From these results in Table V we can see that these deviations of the MC q_x predictions are higher for harder interactions (attractive or repulsive) and smaller for moderate interaction strengths for both situations considered for the gas-gas interactions [(1) purely repulsive and (2) gas-gas equal to the gas-wall interactions].

If we do not import the accommodation coefficients from the dilute gas simulations, and we just compute them from the temperature profiles for a dense gas, disregarding thus the effect of the density oscillations, we find different values for α_T. These α_T coefficients are computed exactly near the (warm) wall of the channel. For instance, for the case of repulsive wall interactions (tsLJ1.0), α computed from the temperature profiles in Fig. 8 is 0.21. In the same way we compute the accommodation coefficient based on heat fluxes. In Table VI we give all these accommodation coefficients (α_T and α_{q_x}) derived from explicit MD simulations of a dense gas where gas-gas interactions are equal to the gas-wall interactions, together with the q_x results using these coefficients in MC with Maxwell-like B.C. based on α. Analyzing the results from Table VI we see that we get good predictions for q_x^{MC} when using α_T for attractive potentials (hydrophilic interactions), but large deviations are registered for very hard repulsive potentials (tsLJ potential: $\epsilon_{G\text{-}G} = \epsilon_{G\text{-}W} = 1.0$). For a dense gas, the deviations from MD for the $q_x^{\text{MC}}(\alpha_{q_x})$ are much larger than the deviations of $q_x^{\text{MC}}(\alpha_T)$, while for a dilute gas these deviations were similar. From these results we can see that we can get quite accurate results for the heat flux by computing α from T profiles of a dense gas, for all the values of the gas-gas and gas-wall interactions except for the high repulsive interactions.

In this situation, the clustering effect becomes important and the increased collisions near the wall cannot be reflected only in the accommodation coefficient computed immediately at the wall interface. Thus, for this case, we compute α_T for the repulsive interactions not exactly at the wall but at two molecular diameters away from the wall; that means exactly where the clustering effect and the density oscillations disappear. From the temperature profiles of the impinging and reflected molecular fluxes, at the distance of two molecular diameters (see Fig. 8), we find that $\alpha_T = (T_{L(w)} -$

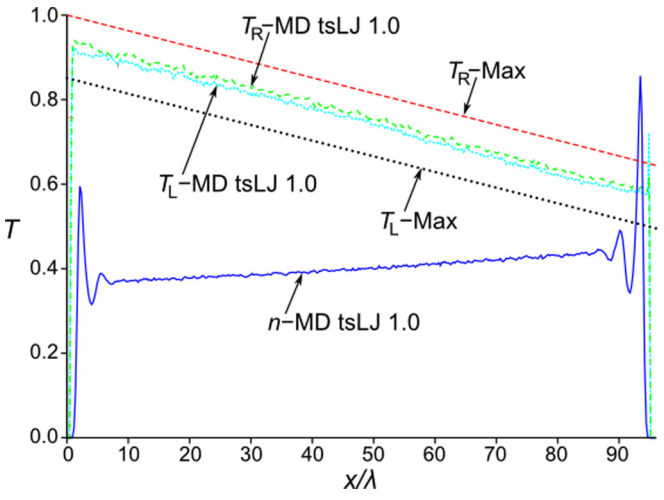

FIG. 8. (Color online) Temperature of the incident and reflected molecules, and total density profiles from MD with explicit and repulsive wall interactions (tsLJ $\epsilon_{G\text{-}S} = 1.0$). Temperature is normalized with T_1 and density with $n_0 = 0.4$ for a system with $\eta = 0.2$.

TABLE VI. Accommodation coefficients for all the gas-gas and gas-wall interactions (column 1) computed from the temperature profiles (α_T) and heat fluxes (α_{q_x}) for a dense gas with $\eta = 0.2$ and $L_x = 95\lambda$ (column 2 and 3). Based on these coefficients are computed the heat fluxes $q_x(\alpha_T)$ (column 4) and $q_x(\alpha_{q_x})$ (column 5) using MC with Maxwell-like B.C. based on α_T and α_{q_x}. Column 6 contains the explicit MD heat flux ${q_x}^{\mathrm{MD}}$. Columns 7 and 8 contain the deviations of the MC heat flux from the MD results.

$\epsilon_{G\text{-}G} = \epsilon_{G\text{-}W}$	α_T	α_{q_x}	$q_x(\alpha_T)$	$q_x(\alpha_{q_x})$	${q_x}^{\mathrm{MD}}$	$dev1$	$dev2$
tsLJ 1.0	0.18	0.75	0.0121	0.0202	0.0148	0.18	0.36
LJ 0.10	0.15	0.60	0.0106	0.0191	0.0104	0.01	0.84
LJ 0.25	0.17	0.71	0.0120	0.0203	0.0123	0.02	0.65
LJ 0.50	0.25	0.94	0.0140	0.0209	0.0148	0.05	0.41

$T_{R(2a)})/(T_{L(2a)} - T_{R\mathrm{Max}(2a)}) = 0.25$. The MC predicted heat flux is then $q_x^{\mathrm{MC}}(\alpha_T) = 0.014$ and the deviations from the MD heat flux q_x^{MD} is $dev = [q_x^{\mathrm{MD}} - q_x^{\mathrm{MC}}(\alpha_T)]/q_x^{\mathrm{MD}} = 0.05$. We see that even if the temperature of the reflected molecules does not describe their collision with the wall anymore, the values of heat fluxes predicted from the temperature profiles are in this case more accurate than in the case of computing it exactly near the wall.

In MD, the gas-gas interactions play an important role even when we have thermal wall B.C. (Maxwell with $\alpha = 1$) when $\eta = 0.2$ and they determine different properties for these molecular fluxes (temperature and total q_x). How these MD properties vary with the gas-gas interactions, both for explicit gas-wall interactions and for thermal gas-wall B.C. (Maxwell with $\alpha = 1$), we can find in Table VII. In Table VII we give the temperatures near the warm wall of the incident and reflected molecules (T_L and T_R), and also the total heat flux q_x for all the G-G and G-W interactions. The first four rows contain the values of these properties in the case of thermal B.C. (Maxwell with $\alpha = 1$) and the last four rows in the table contain the values for the same properties but in the case of explicit gas-wall interactions. The explicit gas-gas interactions are modeled in MD using tsLJ and LJ potential with different parameters and interaction strengths. If we consider that the difference in the temperature between the incident and the reflected molecules is a measure of the boundary thermal accommodation, we notice that Maxwell overestimates this thermal accommodation comparing with the explicit simulations results. Moreover, for Maxwell gas-wall B.C. the difference in the temperature of these molecular fluxes is increasing with the gas-gas interactions, while for the explicit gas-wall and gas-gas interactions this relation is not valid. For explicit simulations, the difference between these fluxes is the result of the complex overlapping effect of gas-gas, gas-wall, and clustering effect. In this case the heat flux q_x is high for very attractive or very repulsive interactions and lower for moderate interaction strengths.

TABLE VII. Properties of the molecular fluxes for a dense gas with $\eta = 0.2$, $L = 95\lambda$, depending on different gas-wall interactions (column 1) and gas-gas interactions (column 2). The first four rows correspond to the Maxwell gas-wall B.C ($\alpha = 1$) and the last four rows correspond to explicit gas-wall interactions described by the given LJ and tsLJ potential. Column 3 contains the temperature of the reflected molecules, column 4 of the impinging molecules, and column 5 contains the total heat flux between the two walls.

G-W	G-G	T_R	T_L	q_x
Max	tsLJ 1.0	1.0	0.974	0.020
Max	LJ 0.10	0.996	0.967	0.017
Max	LJ 0.25	0.989	0.952	0.017
Max	LJ 0.50	0.973	0.910	0.016
tsLJ 1.0	tsLJ 1.0	0.930	0.915	0.015
LJ 0.10	LJ 0.10	0.903	0.886	0.010
LJ 0.25	LJ 0.25	0.925	0.910	0.013
LJ 0.50	LJ 0.50	0.944	0.927	0.015

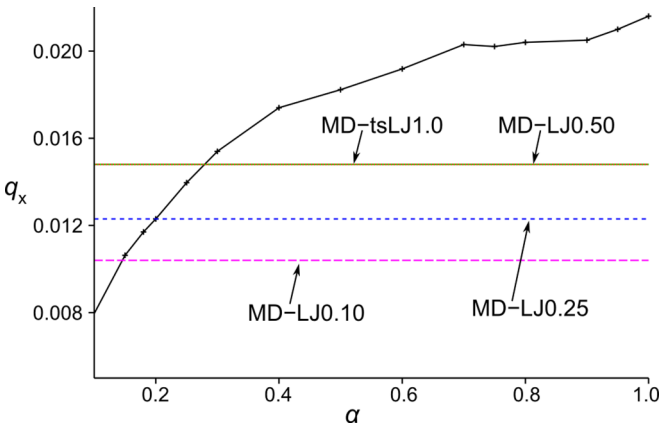

FIG. 9. (Color online) MC heat flux predictions as a function on accommodation coefficient α (Maxwell-type boundary conditions) with continuous lines. Comparison with MD heat prediction for different gas-wall interactions ($\epsilon_{\mathrm{LJ}} = 0.10$, $\epsilon_{\mathrm{LJ}} = 0.25$, $\epsilon_{\mathrm{LJ}} = 0.5$, and $\epsilon_{\mathrm{tsLJ}} = 1.0$). The heat flux both in MD and MC is normalized with the reference heat flux q_0, and a dense gas is considered with $\eta = 0.2$.

As α is not reliable for hydrophilic wall interactions, an effective map (see Fig. 9) is used to determine the effective accommodation coefficients. This is showing the dependence on a generic α of the heat flux predictions when using MC with Maxwell-like B.C. In this map, for a certain heat flux prediction in MD we can obtain the corresponding α that will give the expected heat flux prediction using MC with Maxwell-like B.C.(α).

In the end, we compare these accommodation coefficients found until now from the T profiles with the effective accommodation coefficients found by matching the explicit MD heat fluxes (q_x^{MD}) with the map of the q_x^{MC} dependence on the accommodation coefficient α in Fig. 9. As we have computed all these explicit MD heat fluxes for all the gas-gas and gas-wall interactions, we can easily now estimate the effective values of the accommodation coefficients. Here we give the example again for the case when the gas-gas interactions are equal to the gas-wall interactions (in LJ: $\epsilon_{G\text{-}G} = \epsilon_{G\text{-}W} = 0.10,0.25,0.50$; for tsLJ: $\epsilon_{G\text{-}G} = \epsilon_{G\text{-}W} = 1.0$). The accommodation coefficients α_T computed from the explicit MD simulations for all the gas-gas and gas-wall interactions and the effective accommodation derived from Fig. 9 are found in Table VIII. We find that these MD coefficients are very close

TABLE VIII. Accommodation coefficients α_T computed from the temperature of the impinging and reflected molecules for a dense gas with $\eta = 0.2$ (column 3) and the effective accommodation coefficients derived from the MC heat flux dependency on a generic α (column 2), for all the hydrophilic (LJ: $\epsilon_{G\text{-}G} = \epsilon_{G\text{-}W} = 0.25, 0.50$) and hydrophobic interaction strengths (tsLJ: $\epsilon_{G\text{-}G} = \epsilon_{G\text{-}W} = 1.0$; LJ: $\epsilon_{G\text{-}G} = \epsilon_{G\text{-}W} = 0.10$).

$\epsilon_{G\text{-}G} = \epsilon_{G\text{-}W}$	α_{q_x}	α_T
tsLJ 1.0	0.25	0.25
LJ 0.10	0.14	0.15
LJ 0.25	0.20	0.17
LJ 0.50	0.28	0.25

to the effective coefficients for all the gas-gas and gas-wall interactions considered.

V. HEAT FLUX DEPENDENCE ON MOLECULAR PARAMETERS

Another two important parameters in energy exchange during collisions in the gas-surface interface are the molecular fluid-wall mass and radius ratios. In all the previous MD simulations, we considered the mass and radius of the gas molecules equal to the mass and radius of the molecules in the solid. In the following sections we are looking at the effect on the heat flux q_x and on the accommodation coefficient α for different fluid-wall mass and radius ratios.

A. Heat flux as a function on gas-wall mass ratio

In [19], heat flux and temperature of the molecular fluxes were computed for four gas-wall mass ratios and for four interaction strengths. Here we compute these quantities for eight mass ratios and we compute the accommodation coefficients based on different properties (T, q_x, etc.). We investigate if the accommodation coefficients are more sensitive to the interaction strength or to the gas-wall mass ratios and we determine the function dependency of α on (m_1/m_2).

We look first at the dependency of the MD heat flux predictions (q_x^{MD}) on the molecular gas-wall mass ratio. The same molecular model is used as previously described. As the values of the accommodation coefficient computed from the energy (q_x) and from the temperature T of the impinging and reflected molecular fluxes give the most accurate results for the total heat flux predictions when compared to MD results (see previous section), we use these definitions to compute α_{q_x} and α_T for different gas-wall mass ratios and for different gas-surface interaction strengths. More values of the heat fluxes for different gas-wall mass ratios are shown in Table IX for both hydrophilic and hydrophobic wall interactions. We see here that α_{q_x} and α_T are increasing with $\epsilon_{G\text{-}W}$ for a fixed gas-wall mass ratio and are decreasing with increasing the gas-wall mass ratio for a fixed $\epsilon_{G\text{-}W}$.

The gas-wall attraction seems to have a higher impact on α_{q_x} and α_T than the gas-wall mass ratio (e.g., in Table IX, α is changing from 0.67 for attractive walls with $\epsilon = 0.5$ to 0.22 for repulsive wall interactions with $\epsilon = 1.0$). For very low gas masses, α is very small. This is explainable as that fast moving particles will hardly be influenced by the wall and are expected to bounce elastically. In Table X we can compare α_{q_x} for two more values of the interaction strengths ($\epsilon_{G\text{-}W} = 0.1$ and $\epsilon_{G\text{-}W} = 0.25$) and for two more gas-wall mass ratios. We see again that α is varying more on the columns (different strengths of the interactions ϵ) than on the lines (different gas-wall mass ratios).

TABLE IX. Average heat flux and accommodation coefficient for different molecular gas-wall mass ratios m_1/m_2 for a dilute gas with $\eta = 0.005$. The values are given for $\epsilon_{\mathrm{LJ}} = 0.50$ and $\epsilon_{\mathrm{tsLJ}} = 1.0$.

$\epsilon_{\mathrm{LJ}} = 0.50$				$\epsilon_{\mathrm{tsLJ}} = 1.0$			
m_1/m_2	q_x^{MD}	α_{q_x}	α_T	m_1/m_2	q_x^{MD}	α_{q_x}	α_T
1.0	0.0011	0.67	0.65	1.0	0.000 49	0.22	0.13
0.75	0.0014	0.70	0.66	0.75	0.000 62	0.23	0.18
0.50	0.0018	0.78	0.71	0.50	0.000 76	0.24	0.16
0.37	0.0019	0.71	0.66	0.37	0.000 87	0.24	0.15
0.25	0.0022	0.68	0.64	0.25	0.00100	0.23	0.15
0.12	0.0024	0.52	0.50	0.12	0.000 89	0.14	0.10
0.06	0.0023	0.35	0.36	0.06	0.000 75	0.09	0.07
0.03	0.0022	0.24	0.25	0.03	0.000 50	0.04	0.04

From the results for both α_T and α_{q_x} as a function of gas-wall mass ratio in Table IX, we find that the value of the accommodation coefficient has a maximum around gas-wall mass ratio 0.6 both for hydrophilic and hydrophobic wall interactions. Also we see that α doesn't vary too much when having higher mass ratios, but varies quite fast at small mass ratios. From these results we see again that we have a maximum thermal accommodation when the gas-wall mass ratio is around 0.6.

B. Heat flux as a function on gas-wall radius ratio

Another parameter that influence the heat flux q_x is the gas-wall radius ratio. In Table XI we find the data for hydrophilic ($\epsilon_{\mathrm{LJ}_{G\text{-}W}} = \epsilon_{\mathrm{LJ}_{G\text{-}G}} = 0.5$) and hydrophobic wall interactions ($\epsilon_{\mathrm{tsLJ}_{G\text{-}W}} = \epsilon_{\mathrm{tsLJ}_{G\text{-}G}} = 1.0$). From these tables we see different behavior for hydrophilic-hydrophobic wall interactions function on gas-wall radius ratio. For hydrophilic wall interactions, α has a local minimum and maximum depending on the gas-wall radius ratio and for hydrophobic wall interactions α is increasing with decreasing the gas-wall radius ratio.

If the gas-wall radius ratio r_1/r_2 is small, then the gas particles are much smaller than the wall particles and the gas

TABLE X. Accommodation coefficients for different molecular gas-wall mass ratios m_1/m_2 and different values of ϵ in the Lennard Jones potential (hydrophilic wall) or in the truncated shifted Lennard Jones (hydrophobic wall) for a dilute gas with $\eta = 0.005$.

ϵ	$m_1/m_2 = 1.0$	$m_1/m_2 = 0.125$
LJ: 0.5	0.67	0.43
LJ: 0.25	0.50	0.31
LJ: 0.1	0.22	0.12
tsLJ: 1.0	0.22	0.12

TABLE XI. Average heat flux and accommodation coefficient for different molecular gas-wall radius ratios r_1/r_2 for a dilute gas with $\eta = 0.005$. The values are given for $\epsilon_{\mathrm{LJ}_{G\text{-}G}} = \epsilon_{\mathrm{LJ}_{G\text{-}W}} = 0.50$ and for $\epsilon_{\mathrm{tsLJ}_{G\text{-}G}} = \epsilon_{\mathrm{tsLJ}_{G\text{-}G}} = 1.0$.

$\epsilon_{\mathrm{LJ}} = 0.50$				$\epsilon_{\mathrm{tsLJ}} = 1.0$			
r_1/r_2	q_x^{MD}	α_{q_x}	α_T	r_1/r_2	q_x^{MD}	α_{q_x}	α_T
0.25	0.00161	0.78	0.75	0.25	0.00101	0.48	0.24
0.50	0.00172	0.71	0.72	0.50	0.000 76	0.35	0.23
0.75	0.00141	0.68	0.71	0.75	0.000 64	0.29	0.22
1.00	0.00114	0.72	0.70	1.00	0.000 45	0.20	0.15
1.50	0.000 57	0.78	0.72	1.50	0.000 36	0.16	0.16
2.00	0.000 45	0.99	0.79	2.00	0.000 22	0.00	0.00

molecule for attractive wall interactions can be incorporated in the wall generating thus a high accommodation coefficient α. If the gas-wall radius ratio r_1/r_2 is large, then the large gas molecules colliding with the wall interact actually with more than one wall molecule per collision. So, if the gas-wall interactions are attractive, then the accommodation coefficient is very high, and if the gas-wall interactions are repulsive, then the accommodation coefficient is very low (almost zero). The gas molecule in this case sees the wall as a smooth plane rather than a molecular wall.

It is interesting to see that for attractive walls (hydrophilic), we have high accommodation coefficients for both very small and very high gas-wall radius ratios (e.g., gas and wall molecular radius are very different from each other). When these gas-wall radius ratios are around 1 (gas molecular radius is equal to wall molecular radius), α registers local minimum values as shown in Table XI, columns 2, 3, and 4.

For hydrophobic wall interactions, the higher the gas-wall radius ratio, the higher the repulsion to the wall and the smaller the accommodation coefficient α. The heat flux in this case is decreasing with the gas-wall radius ratio (see Table XI, columns 6, 7, and 8).

VI. ACCOMMODATION COEFFICIENT OF AN ARGON AND XENON GAS ON A PLATINUM SURFACE. COMPARISONS WITH EXPERIMENTAL RESULTS

These generic results on accommodation coefficients are used to predict the thermal accommodation for realistic systems. We consider further two situations: (a) an argon gas confined in a channel having platinum walls and (b) a xenon gas in a channel having platinum walls. For these two systems the fluid-wall mass and radius ratios are the following: (a) $m_{\mathrm{Ar}}/m_{\mathrm{Pt}} = 0.20$, $r_{\mathrm{Ar}}/r_{\mathrm{Pt}} = 1.35$; (b) $m_{\mathrm{Xe}}/m_{\mathrm{Pt}} = 0.67$, $r_{\mathrm{Xe}}/r_{\mathrm{Pt}} = 1.62$. Taking into account our previous results, we can predict that xenon on platinum has a higher accommodation coefficient α because the gas-wall mass and radius ratios is closer to the optimal combination corresponding to gas-wall mass ratio around 0.6 and gas and wall radius different from each other.

We compute the accommodation coefficients from the MD simulations and we compare them with the accommodation coefficients obtained from the energy [17] and with the experimental results [26,27].

We consider thus the same parameters for the gas-wall interactions as considered by Yamamoto [11]. Yamamoto used Morse potential to describe the Pt-Xe and Pt-Ar gas-wall interactions:

$$V_{M_{\text{Xe-Pt}}} = \epsilon_{\text{Xe-Pt}}\{\exp[2\sigma_{\text{Xe-Pt}}(x - r_{0_{\text{Xe-Pt}}})] - 2\exp[-\sigma_{\text{Xe-Pt}}(x - r_{0_{\text{Xe-Pt}}})]\},$$

$$V_{M_{\text{Ar-Pt}}} = \epsilon_{\text{Ar-Pt}}\{\exp[-2\sigma_{\text{Ar-Pt}}(x - r_{0_{\text{Ar-Pt}}})] - 1\}^2,$$

with the following parameters for Ar-Pt: $\epsilon_{\text{Ar-Pt}}/k_b = 134.7$ K, $\sigma_{\text{Ar-Pt}} = 1.6$ Å^{-1}, and $r_{\text{0-Ar-Pt}} = 4.60$ Å^{-1}; for Xe-Pt: $\epsilon_{\text{Xe-Pt}}/k_b = 319.1$ K, $\sigma_{\text{Xe-Pt}} = 1.05$ Å^{-1}, and $r_{0_{\text{Xe-Pt}}} = 3.20$ Å^{-1}.

The units for our MD simulations are expressed in reduced units consisting of the unit of length (σ^*), the unit of mass (m^*), and the unit for energy ϵ^* as previously described in Sec. II. The mass and the size of wall particles (platinum) are here as well taken as unity. The walls are kept together by a relatively strong interaction strength $\epsilon_{\text{Pt-Pt}} = 6\epsilon^*$ in the potential function.

When converting the Morse parameters to the units of our MD simulations [18] [ϵ^*,σ^*], where $\epsilon^*/k_b = 628.58$ K and $\sigma^* = 2.523$ Å, we get the following set of parameters for the Morse potential expressed in MD units: $\epsilon_{\text{Ar-Pt}}/k_b = 0.2132\epsilon^*$, $\sigma_{\text{Ar-Pt}} = 4.036\sigma^{*-1}$, $r_{0\text{Ar-Pt}} = 1.82\sigma^*$ for Ar-Pt; for Xe-Pt: $\epsilon_{\text{Xe-Pt}}/k_b = 0.5076\epsilon^*$, $\sigma_{\text{Xe-Pt}} = 2.649\sigma^{*-1}$, $r_{0\text{Xe-Pt}} = 1.268\sigma^*$. The temperatures of the walls are $T_1 = 0.7159[\epsilon^*/k_B] = 450$ K and $T_2 = 0.4772[\epsilon^*/k_B] = 300$ K.

As our MD model is based on the LJ potential, we first find the parameters of the Lennard-Jones potential that best fit the Morse potential as considered by Yamamoto [17]. When fitting these potentials in terms of [ϵ_{Pt},σ_{Pt}] units we find the following parameters for the Lennard-Jones potential to describe the gas-surface interactions in the case of Ar and Xe on Pt (see Fig. 10).

The derived set of parameters for the Lennard Jones potential is $\epsilon_{\text{Xe-Pt}} = 0.5076\epsilon^*$ ($\epsilon_{\text{Xe-Pt}}/k_b = 319.1$ K), $\sigma_{\text{Xe-Pt}} = 1.13\sigma^{*-1}$ and $\epsilon_{\text{Ar-Pt}} = 0.2132\epsilon^*$ ($\epsilon_{\text{Ar-Pt}}/k_b = 134.7$ K), $\sigma_{\text{Ar-Pt}} = 1.62\sigma^{*-1}$.

These parameters are used to getting the temperature profiles and heat fluxes of the impinging and reflected molecules, both for an argon and for a xenon gas on a platinum surface. From the temperature profiles in the channel the accommodation coefficients α are computed and compared with the values obtained by Yamamoto [17] and by experimental results [26,27] (see Table XII). We see that these values compare very well with the ones from Yamamoto's model, but even better with the experimental values. Moreover, our generic MD simulations showed good qualitative predictions for the thermal accommodation, indicating higher α_T for Xe on Pt as confirmed also by the explicit MD results of the system and by the other numerical and experimental results [17,26,27].

VII. ERROR ESTIMATION FOR THE COMPUTED ACCOMMODATION COEFFICIENTS

In all previous sections, the accommodation coefficients were reported for different systems using the MD method. Here we give an indication about the accuracy of the computed

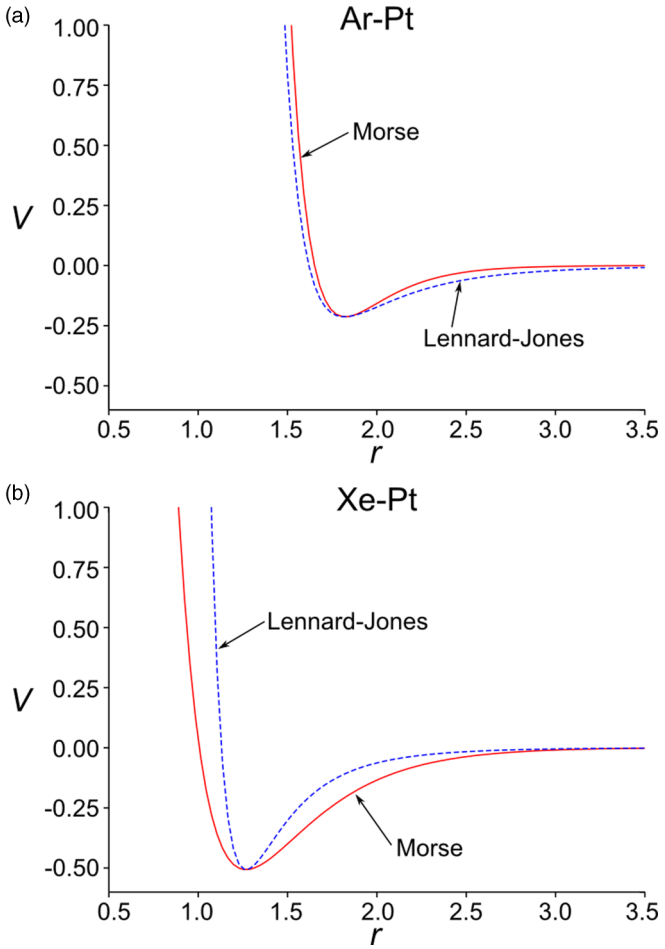

FIG. 10. (Color online) Fitted Lennard Jones potential to match the Morse potentials with the parameters given in the text for (a) Ar gas on Pt surface and (b) Xe gas on Pt surface.

accommodation coefficients both from temperatures and heat fluxes, for all the independent situations studied. As a summary, these included generic low density systems ($\eta = 0.005$) with different gas-wall interactions and different gas-wall mass ratios, high density systems ($\eta = 0.2$) and real systems like argon and xenon gas in a platinum wall channel.

The accuracy of the temperature and heat flux profiles consisted in the number of samples considered for the final averaging. As an example, for the Pt-Ar and Pt-Xe system,

TABLE XII. Comparison of accommodation coefficients computed using different methods for a dilute gas with $\eta = 0.005$. The first line contains the values of α's for a Xe gas on a Pt surface computed using the energy-tangential momentum accommodation (Yamamoto model), from the temperature profiles in explicit MD simulations, and from experimental results reported in the literature. The second line is for a Xe gas on Pt and the fields have the same significance as in line 1.

	Yamamoto	MD explicit	Experimental
$\alpha_{\text{Xe-Pt}}$	0.85/0.88	0.84	0.85
$\alpha_{\text{Ar-Pt}}$	0.43/0.62	0.58	0.55

TABLE XIII. Standard deviations for the accommodation coefficients computed based on q_x in Ar-Pt and Xe-Pt systems.

α	stdev(α_{q_x})
Xe-Pt	0.0001
Ar-Pt	0.0002

the MD simulation consisted of 10 million iterations and the averaged profiles were done over the last few million iterations. The profiles were very accurate (stdev = 0.0002) and they were used to fit the linear profile through the MD bulk averaged profiles. For the situations where the profiles had large peaks near the walls (as in the case of attractive wall interactions), the accuracy of the accommodation coefficients depends actually on the accuracy of this linear fit through the middle bulk MD points. The accuracy of the fit determines the accuracy of determining $T_{\text{in}}, T_{\text{out}}, q_{\text{in}}, q_{\text{out}}$. In case these peaks are dominant [e.g., $\epsilon_{G\text{-}W} = 0.5$ in Fig. 3(c)], this results in higher errors for the fit and consequently for the accommodation coefficients. An estimation of the standard deviations for all the considered simulations is given in Tables XIII–XV.

In Table XIII we have the standard deviations for the accommodation coefficients computed from the MD heat flux profiles for the Ar-Pt and Xe-Pt systems. The deviations are very small and enhance our conclusion that the accommodation coefficients computed from MD compare very well with experimental and other existing numerical models (see Table XII).

In Table XIV we compare the standard deviations of the accommodation coefficients based on the MD temperature profiles for all the gas-wall mass ratios ($m_{\text{gas}}/m_{\text{wall}} = 0.5$, 0.25, 0.125, 1.0) and for all the gas-wall interactions (tsLJ $\epsilon_{G\text{-}W} = 1.0$; LJ $\epsilon_{G\text{-}W} - 0.1, 0.25, 0.5$). The maximum standard deviation is around 0.0287. In general, these errors are higher for the simulations with highly attractive walls (where there are peaks and jumps in the MD profiles near the walls) and smaller for repulsive wall interactions (tsLJ $\epsilon_{G\text{-}W} = 1.0$). The standard deviations tend to be smaller also for smaller gas-wall mass ratios than for higher mass ratios also due to the presence of the peaks near the walls (see Table XIV).

The accommodation coefficients computed from the heat fluxes for both $\eta = 0.005$ and $\eta = 0.2$ for repulsive wall interactions (tsLJ, $\epsilon_{G\text{-}W} = 1.0$) are given in Table XV. The statistical errors in the case of α's computed from q_x are smaller than for α's computed from the T profiles. For dense systems, the standard deviations for α_T can reach 0.021 in value.

TABLE XIV. Standard deviations for the accommodation coefficients computed based on the MD temperature profiles for all the gas-wall mass ratios and for all the gas-wall interactions (tsLJ $\epsilon_{G\text{-}W} = 1.0$; LJ $\epsilon_{G\text{-}W} = 0.1, 0.25, 0.5$).

	stdev(α_T)			
$m_{\text{gas}}/m_{\text{wall}}$	tsLJ 1.0	LJ 0.1	LJ 0.25	LJ 0.5
0.5	0.0076	0.0145	0.0216	0.0287
0.25	0.0070	0.0115	0.0183	0.0255
0.125	0.0122	0.0108	0.0169	0.0287
1.0	0.0116	0.0141	0.0155	0.0277

TABLE XV. Standard deviations for the accommodation coefficients computed based on q_x and T for dilute ($\eta = 0.005$) and dense systems $\eta = 0.2$. In both situations the gas-wall interactions were tsLJ, $\epsilon_{G\text{-}W} = 1.0$.

η	stdev (α_{q_x})	stdev (α_T)
0.2	0.0002	0.021
0.005	0.0001	0.011

VIII. CONCLUSIONS

In this paper, MD simulations including explicit walls were conducted to study the gas-surface interface, and to compute the effective accommodation coefficients to be used as boundary conditions in MC simulations.

For a dilute gas ($\eta = 0.005$), we find that the accommodation coefficient computed from the heat fluxes give the most accurate heat predictions when compared to explicit MD simulations. Maxwell-like boundary conditions based on α_{q_x} give good results for the total heat flux q_x, both for hydrophilic and hydrophobic wall interactions.

For a dense gas, the gas-gas interactions become dominant and using α_{q_x} computed in the dilute gas simulations with the same gas-gas and gas-wall interactions give large deviations for the heat flux predictions when compared to explicit MD results. The accommodation coefficient $\alpha_{q_x}^{\mathrm{MD}}$ computed from the gas-surface interface of a dilute gas and exported to a dense gas gives good results for hydrophobic but not for hydrophilic wall interactions due to the overlapping of attractive wall and clustering effect for this second case. We see that in this case, we can get accurate results for the heat fluxes considering α computed from the T profiles rather than from the q_x, for all the interactions except the high repulsive ones. For repulsive interactions, α_T is computed at two molecular diameters away from the wall (the distance where the clustering effect and the density oscillations disappear) rather than immediately near the wall.

The effect of the interaction strength (ϵ), the fluid-wall mass ratio (m_1/m_2), and radius ratio (r_1/r_2) on the heat flux q_x is characterized. The optimal thermal accommodation coefficient is found for the fluid-wall mass ratio around 0.62 and for the case when the gas-wall radius is either high or small in value (large difference between the gas and wall molecular sizes). The experimental results for xenon and argon on platinum confirm these results. The accommodation coefficient α computed from MD compare very well with experimental and with other numerical molecular model results for thermal accommodation.

[1] R. R. Schmidt and B. Notohardjono, IBM J. Res. Dev. **46**, 739 (2002).

[2] G. Bird, *Molecular Gas Dynamics and the Direct Simulation of Gas Flows* (Clarendon, Oxford, 1994).

[3] A. Kucaba-Pietal and Z. Zbigniew Walenta, Int. J. Turbulence **10**, 77 (2004).

[4] D. Frenkel and B. Smit, *Understanding Molecular Simulation* (Academic Press, San Diego, 1996).

[5] C. Cercignani and M. Lampis, Transp. Theory Stat. **1**, 101 (1971).

[6] M. Cieplak, J. Koplik, and J. Banavar, Physica A **274**, 281 (1999).

[7] R. G. Lord, Phys. Fluids A **3**, 706 (1991).

[8] H. Y. Wachman, in *Rarefied Gas Dynamics: Progress in Astronautics and Aeronautics*, edited by A. R. Seebass (AIAA, Washington DC, 1993), Vol. 158, p. 461.

[9] F. Devienne, J. Souquet, and J. Roustan, in *Rarefied Gas Dynamics: Advances in Applied Mechanics, Suppl. 3*, edited by J. H. Leeuw (Academic, New York, 1966), Vol. 2, p. 584.

[10] J. Gregory and P. Peters, in *Rarefied Gas Dynamics*, edited by V. Boffi and Cercignani (Academic, New York, 1986), Vol. 1, p. 644.

[11] K. Yamamoto, H. Takeuchi, and T. Hyakutake, Phys. Fluids **18**, 046103 (2006).

[12] J. Matsui and Y. Matsumoto, in *Rarefied Gas Dynamics: Progress in Astronautics and Aeronautics*, edited by A. R. Seebass (AIAA, Washington DC, 1993), Vol. 158, p. 515.

[13] N. Yamanishi and Y. Matsumoto, in *Rarefied Gas Dynamics*, edited by R. Brun *et al.* (Cépaduès-Éditions, Toulouse, 1999), Vol. 1, p. 421.

[14] V. Chirita, B. Pailthorpe, and R. Collins, J. Phys. D: Appl. Phys. **26**, 133 (1993).

[15] T. Kimura and S. Maruyama, in 12th International Heat Transfer Conference, 2002 (unpublished), p. 537.

[16] S. V. Nedea, A. J. H. Frijns, A. A. van Steenhoven, A. J. Markvoort, and P. A. J. Hilbers, Phys. Rev. E **72**, 016705 (2005).

[17] K. Yamamoto, H. Takeuchi, and T. Hyakutake, in *Rarefied Gas Dynamics*, edited by A. D. Ketsdever and E. P. Muntz (AIP, New York, 2003), Vol. 663, p. 1008.

[18] A. J. Markvoort, P. A. J. Hilbers, and S. V. Nedea, Phys. Rev. E **71**, 066702 (2005).

[19] S. V. Nedea, A. J. Markvoort, A. Steenhoven, and P. A. J. Hilbers, J. Heat Transfer **131**, 033104 (2009).

[20] J. Hinchen and W. Foley, in *Rarefied Gas Dynamics, the 4th International Symposium, Toronto*, edited by J. H. Leeuw, Advances in Applied Mechanics, Vol. 2 (Academic Press, New York, 1966), p. 505.

[21] S. Saxena and R. Afshar, Int. J. Thermophys. **6**, 143 (1985).

[22] K. Yamamoto and T. Shiota, in *Rarefied Gas Dynamics, 21st International Symposium, Marseille* (Cepadues-Editions, Toulouse, 1999), p. 397.

[23] A. Frezzotti, Phys. Fluids **9**, 1329 (1997).

[24] A. Frezzotti, J. Mech. B: Fluids **18**, 103 (1999).

[25] A. J. H. Frijns, S. V. Nedea, A. J. Markvoort, A. Steenhoven, and P. A. J. Hilbers, Int. J. Multiscale Comp. Eng. **4**, 391 (2006).

[26] I. Admur, J. McCormack, and H. Pearlman, J. Chem. Phys. **12**, 159 (1944).

[27] W. Mann, Proc. R. Soc. A **146**, 776 (1934).